Corrosion Science

Corrosion monitoring of 321H in contact with a quaternary molten salt for parabolic trough CSP plants

--Manuscript Draft--

Manuscript Number:	CORSCI_2020_1289R1
Article Type:	Full Length Article
Keywords:	Quaternary salt; CSP; Hitec salt; Parabolic-trough technology; Corrosion Monitoring; 321H steel
Corresponding Author:	Teresa de Miguel Gamo Complutense University of Madrid Madrid, Spain
First Author:	V. Encinas-Sánchez
Order of Authors:	V. Encinas-Sánchez
	M.I. Lasanta
	M.T. de Miguel
	G. García-Martin
	F.J. Perez
Abstract:	Corrosive behaviour of steel 321H in contact with a nitrate-nitrite quaternary salt mixture is assessed. EIS measurements were performed under static conditions at 500 ºC for 1000 hours. EIS results showed that corrosion in 321H is controlled by ion transport through the oxide scale and reveals a protective layer mechanism. These results were in line with those obtained by SEM and XRD. The electrochemical study estimated a corrosion rate of 8.9 μm·year -1 what confirms the suitability of 321H steel as a structural material for CSP technology and the enormous potential of the corrosion monitoring system for O&M processes.
Response to Reviewers:	Dear Editor David Young, We greatly appreciate the invaluable comments provided by the reviewers on our manuscript entitled “Corrosion monitoring of 321H in contact with a quaternary molten salt for parabolic trough CSP plants”. We have agreed with all the comments and inputs and have incorporated every suggested change into the revised manuscript. In the revised manuscript, and below, we have comprehensively responded to the specific comments on the original submission modifying the required parts of the manuscript. We hope since every correction suggested by the reviewers have been incorporated into the resubmitted manuscript that it is now acceptable for publication. However, if more changes are necessary, please do not hesitate to request them and it would be our pleasure to complete them. We look forward to your reply, when possible. Thank you very much for your consideration. Sincerely yours, María Teresa de Miguel Gamo, corresponding author. Dear reviewer, Thanks for your valuable comments. We highly appreciate your insightful and helpful review on our manuscript. We have agreed with all the comments and inputs and have incorporated every suggested change into the revised manuscript. In the revised manuscript, and below, we have tried to comprehensively respond to the specific comments on the original submission modifying the required parts of the manuscript. A "Marked Revised Manuscript" have been provided in order to make you easier to track the corrections made based on your comments.

October 15, 2020

Senior Editor, *Corrosion Science*

Dear Editor David Young,

We greatly appreciate the invaluable comments provided by the reviewers on our manuscript entitled "**Corrosion monitoring of 321H in contact with a quaternary molten salt for parabolic trough CSP plants**". We have agreed with all the comments and inputs and have incorporated every suggested change into the revised manuscript. In the revised manuscript, and in the "Detailed Response to Reviewers" document, we have comprehensively responded to the specific comments on the original submission modifying the required parts of the manuscript. We hope since every correction suggested by the reviewers have been incorporated into the resubmitted manuscript that it is now acceptable for publication. However, if more changes are necessary, please do not hesitate to request them and it would be our pleasure to complete them.

We look forward to your reply, when possible.

Thank you very much for your consideration.

Sincerely yours,

María Teresa de Miguel Gamo, corresponding author.

Dept. Chemical and Materials Engineering
Universidad Complutense de Madrid, Madrid, Spain
Phone: (+34) 91 394 5208
E-mail: mtdmiguel@ucm.es

Reviewer #1:

This manuscript has studied the corrosion behaviors of 321 H alloy in LiNO3 contained Hitec salts at 500 degree C by electrochemical method, the results are meaningful for the understanding of the corrosion mechanism of alloy in nitrate molten salts and the development of a low melt point nitrate salt using as thermal storage medium for parabolic CSP plants. However, there are some details should be further discussed before the accepting of this manuscript.

Thanks for your valuable comments. We highly appreciate your insightful and helpful review on our manuscript.

1."Open circle voltage (OCV)" should be "Open circle potential (OCP)"

As suggested, OCV has been replaced by OCP in the manuscript (Page 6, Lines 22; Page 7, Lines 3 and 4).

2. Figure 3, authors pointed out that Nyquist plot consisted of a double capacitance loop, however, the EIS results obtained after 250 h testing time are different from those obtained at 24h, 72h and 168h. It would be more exact to describe the as "Nyquist plot composed of a capacitive loop at high frequency and a line at low frequency (Warburg impedance)". Therefore, the corrosion mechanism for 321 H in nitrate molten salts changed after 250h.

We completely agree with the reviewer´s appreciation that, according Figure 3, the corrosion mechanism is evolving along the time. These researchers had the same impression that the reviewer indicates in the comment, so during the EIS data treatment, data were fitted to different equivalent circuits therefore different corrosion mechanisms.

EIS results after 250 h were fitted to the equivalent circuit for a protective-layer mechanism (Figure A, below) and to an equivalent circuit for a porous layer mechanism (Figure (B) below) that would correspond to a Nyquist composed of a capacitive loop at high frequency and a line at low frequency. The best fitting was obtained for the protective-layer mechanism in all the cases between 250 h and 1000 h of experiment.

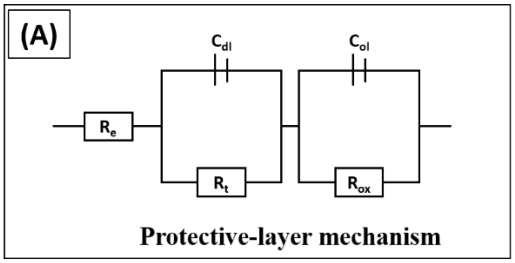

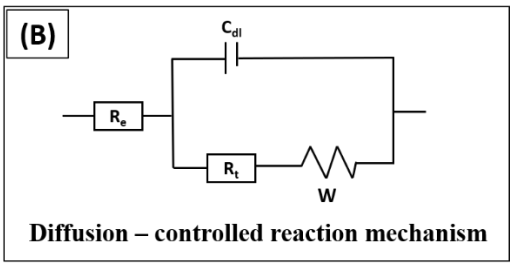

As the reviewer remarks, the second loop seems to be evolving to a line what indicates that the corrosion mechanism is changing. However, during the first 1000 hours of the experiment, the equivalent circuit corresponding to a protective-layer mechanism is still the best model that explains the corrosive process that is taking place. It is supposed that this situation could change if the test were extended to longer time.

3. As pointed out by authors, the corrosion behaviour during the initial stages were quite different from those observed between 168 h and 1000h, it is not suitable to fit the impedance spectral based on a same equivalent circuit shown in Figure 4.

As it has been explained in the previous comment, the best fitting of the electrochemical results was obtained for the equivalent circuit that represents a protective-layer mechanism. As can be seen from Table 2 in the manuscript, even the equivalent circuit is the same, parameters vary from one time to another. For example, the resistance due to the corrosion layer suffer a great decrease when compared the value at the beginning of the experiment (around 71 Ohm) and the end (23 Ohm). These results indicate that the protective behaviour is decreasing what it is coherent with an evolution to a diffusion-controlled mechanism.

4. It is hard to determine the corrosion kinetics following a parabolic law from Figure 6, more evidences are needed.

We completely understand this reviewer´s comment. The concept "parabolic kinetic corrosion law" was incorrectly used in the manuscript, it has been avoided and the paragraph has been modified by explaining the evolution of the corrosion rate along the time.

The paragraph has been modified in the manuscript (Page 14, Lines 8 – 12) as follows:

"The evolution of the corrosion rate (see Fig. 6) presents the highest value at the beginning of the 321H steel exposure to the molten salt. As the corrosion layer grows, it

provides some protection that results in a corrosion rate decrease and ultimately it remains constant. This result is in line with that obtained by Gomes et al. for the corrosion behaviour of 321H steel immersed in Solar Salt [47].”

5. Before the weighing of the corroded samples, had the residual molten salt on the surface of the samples been removed? Or they had been cleaned before the determining of their gravimetric mass?

We thank the reviewer´s comment as we have realized the experimental procedure was not completely clear as it was explained. All the samples are rinsed in a bath of boiling water in order to remove the residual molten salt solidified over the surface. The corresponding paragraph (Page 7, Line 14 - 20) has been modified as follows in order to clarify this section of the experimental procedure:

“Three samples were removed at each selected time and were cooled and rinse with boiling water to remove the remaining salt. The average of their variation weight was considered for the gravimetric results. The formula (Equation 1) used to calculate the mass gain over time was as follows:

$$\frac{\Delta m}{S_0} = \frac{m_f - m_i}{S_0} \qquad (1)$$

where mi is the initial mass of the specimen, mf is the mass of the sample at the selected time and S_0 is the specimen’s initial area.”

6. What is the role of $LiNO_3$ on the corrosion behaviors of 321 H in nitrate molten salts? It should be discussed deeply.

Literature refers that the presence of $LiNO_3$ in molten nitrate - nitrite mixtures induces the corrosion mechanism named “lithiumization”. This mechanism is based in the preferential attack of Li^+ ions to the elements of the steel, specially iron. The higher reactivity of the lithium nitrate, when compared with other alkaline compounds present in the salt (i.e. potassium and sodium nitrates and nitrites), is explained by the higher basicity of this specie.

Several researchers make reference to the presence of lithium oxides, such as $LiFeO_2$ and $LiFe_5O_8$, in the corrosion products when steels are exposed to molten nitrate mixtures containing $LiNO_3$. However, these compounds have not been detected in our study, at least in a crystalline structure. Considering that $LiNO_3$ was present in weight percentages

over 10% in the studies found in literature, it is supposed that 1% $LiNO_3$ addition used in this study is not enough to the lithium oxides development.

This explanation has been included in the manuscript (Page 16, Line 4 – 21) as follows:

"Several researchers have reported lithiumization as one of the main corrosion processes when steels were exposed to nitrate mixtures containing $LiNO_3$ [49, 52-56]. The higher basicity of $LiNO_3$ in comparison with potassium and sodium nitrates suggests that the steels are preferentially attacked by Li^+ ions [56]. The lithiumization mechanism proceeds via (1) to (3) reactions [52, 56]:

$$Fe^{3+}+Li^{+}+2O^{2-}\rightarrow LiFeO_2 \qquad (1)$$

$$6Fe_2O_3+2Li^{+}\rightarrow 2LiFe_5O_8+2Fe^{3+}+2O^{2-} \qquad (2)$$

$$LiFe_5O_8+3Li^{+}\rightarrow 4LiFeO_2+Fe^{3+} \qquad (3)$$

Due to the low atomic number of the lithium, it is not possible to detect it by EDS. Therefore, XRD results were thoroughly analysed in order to assess the presence of lithium oxides. Standard patterns of $LiFeO_2$ and $LiFe_5O_8$, compiled by JCPDS Committee, were compared to the 321H diffraction pattern after molten salt exposure with no success. To the best of the authors knowledge, studies found in literature that reports lithiumization mechanism in nitrate molten salts refers to mixtures with weight percentage in $LiNO_3$ above 10% [49, 52-54]. Based on this fact, it is supposed that the lack of lithium species in this study could be explained by the low content of $LiNO_3$ (1 w%) in the mixture. However, to confirm this hypothesis, it will be needed to perform further studies focused on the lithium concentration in the corrosive media."

Reviewer #2:

1) The paper is well written, concise, well structured, clear and demonstrates the importance of EIS for monitoring corrosion in SS321H when immersed in a mixture of molten salts.

Thanks for your valuable comments. We highly appreciate your insightful and helpful review on our manuscript.

2) The experimental design is reduced in the number of replicates for EIS and the number of test hours (1000h). At least 2000h should be done because this steel is prone to spallation for longer times which can modify the corrosion mechanism. More structural materials should also have been studied/included.

We are completely in agreement with this reviewer's comment. This research was performed in the frame of the European project MSLOOP. Due to time restrictions, associated to the planning of the project, the experimental duration was limited to 1000 hours. However, in the second stage of the study, where the electrochemical monitoring system is scaled up to pilot plant, the exposure time will be extended up to 3000 hours.

On the other hand, more structural materials, mainly ferritic steels and protective coatings, are planned to be studied in this additived Hitec salt in the near future.

3) The corrosion rate was calculated using electrochemical data with 2 replicates. With only 2 replicates and the uncertainty of the method, the value of the corrosion rate should be presented only with 1 decimal place.

We fully agree the reviewer's comment. The value of the corrosion rate, 8,87 µm·year-1, has been replaced by 8,9 µm·year-1, in the manuscript (Page 13, Line 16; Page 17, Line 13 and Table 4 in Page 24).

4) The corrosion rate was calculated using electrochemical data with 2 small replicates. With only 2 replicates and the uncertainty of the method, the value of the corrosion rate should be presented only with 1 decimal place.

We fully agree the reviewer's comment. The value of the corrosion rate, 8,87 µm·year-1, has been replaced by 8,9 µm·year-1, in the manuscript (Page 13, Line 16; Page 17, Line 13 and Table 4 in Page 24)

5) To be proposed as a new quaternary molten salt mixture, more data about this mixture should be submitted. It is known that the introduction of $LiNO_3$ lower the melting point of nitrate salt mixture. However, in this case 1% lowered the melting point of HITEC by 10°C. This decrease in melting point should also be reflected in the degradation temperature, i.e. it should also have a degradation temperature lower than HITEC and not higher, as shown in figure 2b. These data need to be justified.

We really appreciate this reviewer´s comment. In order to show how the $LiNO_3$ addition implies a reduction in the Hitec melting point, DSC curve of the new quaternary mixture is presented in comparison with that corresponding to pure Hitec salt (Figure 2a (Page 26). The experimental results showed a decrease in the melting point of 9 ºC instead of 10 ºC. This data has been modified in the manuscript (Page 8, Line 22).

On the other hand, according to the reviewer´s comment, the decrease in melting point is indeed reflected in the stability of the salt. Figure 2b (Page 25, Line 3) has been replaced by the TGA curves comparison between Hitec and Hitec + 1% $LiNO_3$ and, it shows that the degradation point reduction, due to the 1% $LiNO_3$ addition, is 13 ºC.

Specifically, the following paragraph including this information, has been included in the Results and Discussion section (Page 8, Line 19 to Page 9, Line 7). Additional bibliography has been added to support the results *[C.Villada, F. Jaramillo, J. G. Castaño, F. Echeverría, F. Bolívar, Design and development of nitrate-nitrite based molten salts for concentrating solar power applications, Solar Energy, 188 (2019) 291-299.][T. Wang, D. Mantha, R. G. Reddy (2013). Novel low melting point quaternary eutectic system for solar thermal energy storage. Applied Energy, 102 (2013) 1422-1429]".*

"DSC analysis was performed to obtain the melting point of the additived Hitec mixture. Figure 2a shows the curve obtained in comparison with the corresponding to pure Hitec salt. According to this curve, the salt mixture melts at 132 ºC, which means that its melting point is 9 ºC below that of Hitec salt (143 ºC)

Regarding the molten salt degradation, the maximum stability temperature was set as the temperature at which 3% of the salt's weight is lost. Based on this criterion, and as it is shown in Figure 2b, the maximum stability temperature of the prepared quaternary salt and Hitec mixture under airflow is 678 ºC and 691 ºC, respectively. These results are in line with the behaviour of the $LiNO_3$ addition found in literature that reveals that the effect of melting point decrease of this compound is also reflected in the degradation temperature [32, 33].

6) The amount of impurities (wt%) of each salt should be indicated.

As suggested, purity of the compounds used to manufacture the additived mixture has been indicated in the manuscript (Page 5, Lines 2 - 3). Moreover, concentration of the

main impurities analysed in the salt (i.e. chlorides, sulphates, etc.) have been collected in Table 1 (Page 24).

Table 1. Impurities concentration in the quaternary molten salt mixture

Hitec + 1%LiNO3					
Chlorides (µg·g-1)	*Sulphates (µg·g-1)*	*Carbonates (µg·g-1)*	*Magnesium (µg·g-1)*	*Aluminium (µg·g-1)*	*Calcium (µg·g-1)*
122 ± 7	*431 ± 43*	*< 600*	*< 1*	*< 1*	*25 ± 2*

7) The methodology should give the minimum information about SEM-EDX and XRD. The equipment used should be indicated as well as the experimental conditions. It does not seem enough to mention 4 references.

We fully understand this reviewer´s comment. Detailed information about SEM-EDX and XRD equipment and analysis conditions has been included in the manuscript (Page 7, Line 21 – Page 8, Line 13)

"The morphology and chemical composition of the corrosion layer was analysed by Scanning Electron Microscopy – Energy Dispersive X-ray spectroscopy (SEM-EDX). The equipment employed was a JEOL® JSM-820 scanning electron microscope operated at 25 kV and equipped with a backscattered electron detector. EDX analysis were carried out with a recommended working distance of 10 mm. X-Ray diffraction (XRD) was performed over the samples to identify the crystalline phases present in the corrosion layer. To this end, a PANalytical® (X'Pert PRO MRD model) diffractometer with copper target ($K_{\alpha 1}$ = 1.54056 Å y $K_{\alpha 2}$ = 1.54439 Å) was used. Analysis were carried out at a voltage of 45 kV and 40 mA of current, with a grazing incidence from 20º and 90º, a step size of 0.05º and 3 seconds of measuring time per step. When grazing incidence XRD analysis was performed, the angle of incidence was of 0.5º.

Standard patterns used for crystalline compounds identification corresponds to those compiled by Joint Committee on Powder Diffraction Standards (JCPDS) Committee. On the other hand, XRD analysis was performed over the substrate, 321H steel, untested and

the quaternary molten salt mixture used in this study. These results were presented jointly with the corroded samples in order to facilitate their identification."

8) Section 2.1.2 The number of replicates for gravimetry should be indicated in this section.

As suggested, the number of replicates for gravimetry have been included in section 2.1.2 (Page 5, Line 21 – Page 6, Line 3) as follows:

"Two different coupons of the 321H stainless steel were prepared. In the case of the EIS measurements, specimens were cylindrical and their dimensions of 50 x 2 mm. Two samples were prepared for the fabrication of a two-electrode corrosion monitoring probe. Test pieces for the gravimetric corrosion test were flat samples of 20×10×2 mm. Three samples were prepared for each measurement time (24, 72, 168, 250, 500, 750, and 1000 hours). Both kind of specimens were superficially grounded with P180 sandpaper and cleaned in distilled water followed by 5 minutes of sonication in ethanol."

9) 3rd paragraph of the methodology. "Additionally…. [30]. This sentence is more suitable for the introduction than for the methodology

We fully agree the reviewer´s assessment. The named paragraph has been moved to Introduction section (Page 4, Line 7 – 17) as follows:

"The studied temperature, 500 ºC, was selected in accordance with the results of the thermal analysis of the salt and temperature restrictions existing in parabolic-trough CSP plants. According to some parabolic-trough plant operators heat losses highly increase when operating above 480-500 ºC [28], 500 ºC being the maximum working temperature at which the thermal losses are assumable. Additionally, due to the parabolic shape of the reflective mirrors, the heat flux in the lower part of the absorber tube is higher than that in the upper part, this leading to a non-uniform temperature distribution and thus generating thermal stresses that are accentuated above 500 ºC. These thermal stresses cause the absorber tube to loss its initial shape, leading to its deviation from the focal line and affecting its optical properties (lower absorption capacity and efficiency) [29]"

10) The value of corrosion rate results should be compared with those obtained with similar salts, namely HITEC and for similar times of exposure (1000h)

We fully understand the reviewer´s comment. Even a deep literature review was performed, it was hard to find studies that analysed 321H steel under the same conditions than those selected in this investigation. Results from 321H steel exposures in commercial salt mixtures (i.e. Solar Salt and Hitec) where temperature and exposure time were close to our study have been gathered in Table 5 (Page 25).

Table 5. Corrosion rate of 321H steel in commercial molten salt mixtures

Steel	*Molten salt*	*Temperature (ºC)*	*Time (h)*	*Corrosion rate (µm·year^{-1})*	*Reference*
321H	*Hitec + 1% LiNO3*	*500*	*1000*	*8,9*	*This study*
321H	*Hitec*	*530*	*2000*	*18*	*[24]*
321H	*Solar Salt*	*500*	*3000*	*7,1*	*[23]*
321H	*Solar Salt*	*550*	*3000*	*9*	*[47]*
321H	*Solar Salt*	*600*	*3000*	*15,9*	*[23]*

Comparison of our corrosion rate results and those found in literature, have been completed as follows (Page 13, Line 14 to Page 14, Line 4):

Table 4 gathers the corrosion rate determined from the EIS test results after 1000 h of testing, including the electrochemical parameters aforementioned, the former being of 8.9 µm·year^{-1}. This value is similar to that measured by Gomes et al. [47], who performed corrosion tests with AISI 321H immersed in a stagnant isothermal mixture of 60% NaNO3 and 40% KNO3 molten salt at 550 °C in atmospheric air, estimating a corrosion rate of 9.0 µm·year^{-1} according to the descaled data. The calculated value is also in the same order of magnitude as Kruizenga and Gill's [23] calculation for this alloy, who obtained a value of 7.1 µm·year^{-1} based on 3064 h of exposure to Solar Salt at 500 ºC. Federsel et al. [24] studied the corrosion behaviour of 321H steel in pure Hitec salt at 530 ºC for 2000 h obtaining an experimental corrosion rate value of 18 µm·year^{-1}. These results, found in the literature and gathered in Table 5, would confirm that the corrosion

behaviour of the additived Hitec is in line with the values registered for the commercial molten salt mixtures.

11) The conclusions say "novel quaternary molten mixture". From the results presented, this statement can not be made.

As suggested, “novel quaternary molten mixture” has been replaced by “studied quaternary molten mixture” (Page 18, Line 4 – 5).

12) Reference [11] delete "gy" on 2nd line

“gy” has been deleted on the manuscript (Page 19, Line 30)

13) Figure 6 - It should be indicated if it is an average or an individual value. With two replicas it should be indicated the two values obtained or the average value, or the minimum and maximum.

We completely agree the reviewer’s comment. The corrosion rate values have been calculated from three independent EIS measurements with the two-electrode probe. As suggested, this clarification has been included in the manuscript (Page 14, Line 5 - 8) as follows:

“The evolution of the corrosion rate over time is gathered in Fig. 6. The corrosion rate values have been calculated as an average from the results of three EIS measurements at each monitored time. Results showed a very low dispersion confirming the measurement stability of the method.”

On the other hand, Figure 6 has been replaced (Page 32) in order to include the error bars, although, due to the low dispersion of the results, these are quite difficult to identify.

Figure 6 caption has been modified as follows, in order to specify that corrosion rate values are an average (Page 23, Line 9):

“Figure 6. Evolution of the average corrosion rate over time for 321H steel in contact with the quaternary salt mixture at 500 ºC for 1000 hours.”

14) Figure 7 - The weight gain data at 1000h is not visible, namely the error bars.

We fully understand the reviewer´s comment and Figure 7 (Page 33) has been modified so the weight gain data and its error bars are visible at 1000 h.

Figure 5 (Page 31) has also been replaced as the same problem in data at 2 h and 1000 h was observed.

15) Figure 8-9 - The images have poor quality and have no indication of how they were obtained (e.g. SE/BSE; beam strength). The image should have better definition and should be characterized.

We are in agreement with reviewer´s comments. The quality of both Figures, 8 and 9, has been improved and the images replaced (Pages 34 and 35, respectively). Figures captions have been completed with the following information:

- Electron detector: both micrographs were taken by means of the backscattered electrons detector

- Beam strength: the voltage of the microscope employed was of 25 kV

Figure caption 8 (Page 23, Line 13) and 9 (Page 23, Line 15) have been changed as follows:

"Figure 8. BSE cross-section image at 25 kV and x5000 magnification. SEM micrographs of a 321H specimen after 1000 hours at 500 ºC.

"Figure 9. BSE cross-section image at 25 kV and x5000 magnification. EDX analysis of a 321H specimen after 1000 hours at 500 ºC.

16) Results of XRD on Bragg-Brentano e grazing-incidence angle geometry (Figure 10-11). For each compound should be included 2<theta> angle and lattice plane (hkl)

As suggested, 2<theta> angle and lattice plane (hkl) of all the crystalline compounds identified by XRD have been gathered in tables. XRD analysis have been performed over the 321H steel untested and the quaternary molten salt. Figure 10 (Page 36) has been modified to include the diffractogram of 321H steel untested. Figure 11 (Page 37) has been modified to include both, 321H steel and quaternary molten salt diffractograms. This will make easier to identify those peaks corresponding to the substrate and molten salts residues in the corroded samples.

Table 6 (Page 25) gathers the parameters, 2<theta> angle and lattice plane (hkl), of each crystalline compound identified by XRD in a 321H specimen after 1000 hours at 500 ºC.

Table 7 (Page 26) gathers the parameters, 2<theta> angle and lattice plane (hkl), of each crystalline compound identified by XRD in a 321H specimen after 168 hours at 500 ºC.

In both cases, reference code of the standard patterns used for the compound identification have been related. These standards have been compiled by Joint Committee on Powder Diffraction Standards (JCPDS) Committee.

Research highlights

- The behaviour of 321H in a Hitec-based quaternary salt mixture salt was studied.
- Electrochemical impedance measurements were performed on the substrate-salt system.
- R_{ox} diminishes sharply, from ~84 Ω to 25 Ω, after the initial stages of the test.
- Electrochemical results led to an estimated corrosion rate of 8.9 $\mu m \cdot year^{-1}$.
- Results confirm the enormous potential of the monitoring system for O&M processes.

Corrosion monitoring of 321H in contact with a quaternary molten salt for parabolic trough CSP plants

V. Encinas-Sánchez, M.I. Lasanta, M.T. de Miguel*, G. García-Martín, F.J. Pérez

Surface Engineering and Nanostructured Materials Research Group, Faculty of Chemical Sciences, Complutense University of Madrid, Complutense Avenue s/n, Madrid, Spain.

Corresponding Author: mtdmiguel@ucm.es

Abstract

In this study, the corrosive behaviour of stainless alloy 321H when in contact with a Hitec-based quaternary salt mixture is assessed. Electrochemical impedance measurements were performed on the substrate-salt system, which was tested under static conditions at 500 ºC for 1000 hours. Results showed that corrosion in 321H is controlled by the ion transport through the oxide scale, and points to the presence of a protective layer mechanism. The fitting parameters showed that R_{ox} diminishes sharply, from ~84 Ω to 25 Ω, after the initial stages of the test. This indicates a reduction in the protective character of the oxide layer formed when the test runs. In addition, after 168 hours of testing, R_t increased slightly, which indicates an increase in the number of species arisen from the substrate to the molten salt. In conclusion, the electrochemical results led to an estimated corrosion rate of 8.87 $\mu m \cdot year^{-1}$ for 321H steel. The results obtained by the corrosion monitoring system were in line with those obtained by Scanning Electron Microscopy and X-Ray diffraction. This study confirms the suitability of 321H stainless steel as a structural material for parabolic trough CSP technology and the enormous

potential of the corrosion monitoring system for O&M processes. The next step is to scale up the proposed system for testing on a demonstration parabolic trough plant.

Keywords: Corrosion monitoring; Quaternary salt; Hitec salt; 321H steel; Parabolic-trough technology; CSP

1. Introduction

In recent years, the promising social, environmental, and economic benefits [1] of renewable energy sources have made them an attractive alternative to fossil fuels. The International Energy Agency (IEA) stated that renewables would account for 40% of the total electricity supply in 2040 [2]. Of the renewable energies available, solar energy has demonstrated great potential, and Concentrated Solar Power (CSP) is a large-scale, commercially viable way to generate electricity [3]. However, although CSP can provide enough clean energy to meet annual global demand, its intermittence presents a technical challenge [1]. The most commercially advanced CSP plants overcome this drawback by using molten salt mixtures as a thermal energy storage (TES) medium [4]. Because of their suitable physical and thermal properties, nitrate salts are currently the fluid implemented for heat storage applications. [5]. Nowadays, a binary mixture commonly called Solar Salt (60wt% $NaNO_3$/40wt% KNO_3) and a ternary salt known as Hitec salt (53wt% KNO_3/7wt% $NaNO_3$/40wt% $NaNO_2$) are the preferred commercially used storage mediums, and they serve as reference salts for numerous studies in the CSP field [6, 7, 8]. However, these salts do have some drawbacks, including weak thermal stability and a high melting point, which means there's room for improvement [9]. Several researchers are searching for new salts with lower melting points and higher thermal stabilities without a considerable increase in corrosive behaviour [10-13]. To this end, numerous compounds such as nitrates ($LiNO_3$ [12], $Ca(NO_3)_2$ [14], etc.) and

nanoparticles (SiO_2 [15], Al_2O_3 [16], etc.) have been added to Solar Salt and Hitec to improve their properties. Of these additives, $LiNO_3$ seems to be a good option because of its ability to improve the range of thermal stability in salts [17]. However, lithium nitrate is more expensive than potassium, calcium, and sodium nitrate [18], which is one of the main reasons why salts with lithium have not yet been used commercially [12]. Despite this, the improved salt properties may outweigh the higher cost by increasing electrical generation and, as a result, reducing the final Levelized Costs of Energy (LCOE) [19, 20].

Because of the salt's composition and the high temperatures it reaches, the corrosion of materials in contact with the molten salt is an important consideration for CSP plants [4]. Materials that are critically vulnerable to molten salt corrosion in thermal storage systems and pipes are made of carbon steel, stainless steel and/or Ni-based alloys, depending on the operating temperature [21]. Grade 321H stainless steel is commonly used as a construction material in CSP plants [22], mainly in parabolic- trough power plants [21]. According to some authors, and as demonstrated by Walczak et al. [21], 321H stainless steel has a corrosion rate of 7.1 μm/year after 3000 hrs of exposure to Solar Salt at 500ºC [23] and 18 μm/year after 2000 hrs of exposure to Hitec salt at 530ºC [24]. Although several studies have been performed to evaluate the corrosive effect of both Solar Salt and Hitec salt on numerous materials, most of them have used conventional techniques, such as microscopy and XRD diffraction [21]. However, to gain a better understanding of the corrosion process a monitoring system that records both, corrosion rates and mechanism, in real-time is desired. Electrochemical impedance spectroscopy (EIS) is regarded as an effective technique for tracking the corrosion evolution of materials in molten salt environments [25, 26]. EIS method bases on assuming that

electrochemical processes occurring among the steels and the ionic fluid can be simulated by simple electrical circuits working under an alternating current [27].

This study, therefore, is focused on assessing the corrosive behaviour of stainless alloy 321H when in contact with the nitrate-nitrite based mixture, Hitec, to which 1%wt. of $LiNO_3$ has been added. To do this, 500 ºC isothermal tests were carried out for 1000 hrs, and the corrosion was monitored using a corrosion monitoring system based on electrochemical measurements. The studied temperature, 500 ºC, was selected in accordance with the results of the thermal analysis of the salt and temperature restrictions existing in parabolic-trough CSP plants. According to some parabolic-trough plant operators heat losses highly increase when operating above 480-500 ºC [28], 500 ºC being the maximum working temperature at which the thermal losses are assumable. Additionally, due to the parabolic shape of the reflective mirrors, the heat flux in the lower part of the absorber tube is higher than that in the upper part, this leading to a non-uniform temperature distribution and thus generating thermal stresses that are accentuated above 500 ºC. These thermal stresses cause the absorber tube to loss its initial shape, leading to its deviation from the focal line and affecting its optical properties (lower absorption capacity and efficiency) [29].

The results obtained by the corrosion monitoring system were supported by other conventional techniques, such as gravimetric assessment and microstructural analysis.

2. Methodology

2.1. Materials

2.1.1. Salt mixture

The chemical compounds used in this study were KNO_3, $NaNO_3$, $NaNO_2$ and $LiNO_3$ (Haifa® 99,4%, BASF® 99%, Quimipur® 99% and Quimipur® 99%, respectively). Main impurities present in the mixture are gathered in Table 1. Based on a Hitec salt composition, a mixture of 53wt.% KNO_3/7wt.% $NaNO_3$/40wt.% $NaNO_2$, to which 1%wt. of $LiNO_3$ was added, was used for this research.

Once prepared, the melting point of the salt mixture and its thermal stability were analysed. These results were taken into consideration when deciding the temperature at which the corrosion tests should be performed. The melting point was determined by differential scanning calorimetry (DSC), using a DSC-Q20 calorimeter. Thermogravimetric analysis (TGA) was employed for thermal stability assessment and the measurement was carried out using a SDT-Q600 equipment. The experimental procedures followed for TGA and DSC analyses were explained in detail in previous published research [4, 30].

Chromium and iron content were analysed in the molten salts once the quaternary mixture was prepared and after 1000 hours of corrosion experiment. Both elements were quantified by ICP-OES using a Perkin Elmer Optima 3300DV equipment.

2.1.2. Substrate

321H steel was the substrate selected for its corrosion evaluation. Its chemical composition in weight percent being 0.08% C, 1.00% Si, 2% Mn, 0.045%P, 0.03% S, 18.00% Cr, 10.00%Ni, 0.35% Ti, and Fe in balance.

Two different coupons of the 321H stainless steel were prepared. In the case of the EIS measurements, specimens were cylindrical and their dimensions of 50 x 2 mm. Two samples were prepared for the fabrication of a two-electrode corrosion monitoring probe. Test pieces for the gravimetric corrosion test were flat samples of 20×10×2 mm. Three

samples were prepared for each measurement time (24, 72, 168, 250, 500, 750, and 1000 hours). Both kind of specimens were superficially grounded with P180 sandpaper and cleaned in distilled water followed by 5 minutes of sonication in ethanol.

2.2. EIS test

Electrochemical impedance spectroscopy (EIS) measurements were performed to monitor the corrosion of 321H steel during 1000 hours of testing immersed in the quaternary molten salt based on 1% $LiNO_3$ additived Hitec. A two-electrode system patented under the reference code WO2017046427 was employed for the EIS monitoring. The detailed description of the experimental setup was provided by these authors in [25] and a sketch of the electrochemical system is shown in Fig. 1. The surface area of each electrodes exposed to the molten salt was 3.14 mm^2.

250 g of the molten salt mixture were placed in an alumina crucible and melted at 180 ºC in an electrical tube furnace (Carbolite®) with atmospheric air. The two electrode – sensor was immersed in the molten salt mixture melted and the whole system was heated up until it reached the required temperature. The working temperature was 500 ºC and was selected in accordance with the thermal analysis of the salt and temperature restrictions, previously explained, existing in parabolic-trough CSP plants.

Once immersed in the salt mixture at 500 ºC, the two electrode - sensor was connected to a potentiostat (VoltaLab 80). The electrochemical impedance measurements were conducted with a sweep frequency from 50 kHz to 10 mHz and the voltage perturbation was applied with an amplitude of 10 mV. EIS experiments were performed at open-circuit potential (OCP) in air and the measurement times were selected on the basis of previous research [3, 4, 6]: 2, 24, 72, 168, 250, 500, 750, and 1000 hours. The first EIS measurement was performed after 2 hours of samples immersion so the electrochemical

system was sufficiently stabilized [31]. The data acquisition was carried out by Voltamaster software while Zview software was employed for impedance data treatment and equivalent electrical circuit fittings. Prior to the EIS measurements, the OCP stability, for at least 30 minutes, was validated, allowing variations of the OCP lower than 10 mV. This condition was essential to check the stability of the molten salts, electrochemical sensor, connections, and the electrochemical cell stability.

2.3. Corrosion test

To support the results obtained by the EIS measurements, previously-cleaned flat 20×10×2 mm specimens were immersed in the melted molten mixture following the same procedure explained for the two electrodes – element in EIS test. The electrical furnace was, in turn, the same used for the electrochemical experiment (Carbolite®)

During the corrosion test, samples were analysed via gravimetric at 0, 24, 72, 168, 250, 500, 750, and 1000 hours to obtain comparable results to the EIS measurements. Three samples were removed at each selected time and were cooled and rinse with boiling water to remove the remaining salt. The average of their variation weight was considered for the gravimetric results. The formula (Equation 1) used to calculate the mass gain over time was as follows:

$$\frac{\Delta m}{S_0} = \frac{m_f - m_i}{S_0} \quad (1)$$

where m_i is the initial mass of the specimen, m_f is the mass of the sample at the selected time and S_0 is the specimen's initial area.

The morphology and chemical composition of the corrosion layer was analysed by Scanning Electron Microscopy – Energy Dispersive X-ray spectroscopy (SEM-EDX). The equipment employed was a JEOL® JSM-820 scanning electron microscope operated

at 25 kV and equipped with a backscattered electron detector. EDX analysis were carried out with a recommended working distance of 10 mm. X-Ray diffraction (XRD) was performed over the samples to identify the crystalline phases present in the corrosion layer. To this end, a PANalytical® (X'Pert PRO MRD model) diffractometer with copper target ($K_{\alpha1}$ = 1.54056 Å y $K_{\alpha2}$ = 1.54439 Å) was used. Analysis were carried out at a voltage of 45 kV and 40 mA of current, with a grazing incidence from 20º and 90º, a step size of 0.05º and 3 seconds of measuring time per step. When grazing incidence XRD analysis was performed, the angle of incidence was of 0.5º.

Standard patterns used for crystalline compounds identification corresponds to those compiled by Joint Committee on Powder Diffraction Standards (JCPDS) Committee. On the other hand, XRD analysis was performed over the substrate, 321H steel, untested and the quaternary molten salt mixture used in this study. These results were presented jointly with the corroded samples to facilitate their identification.

The experimental procedure followed during the corrosion tests and the subsequent sample characterization is well established by the authors and can be found further detailed in [3, 4, 25, 30].

3. Results and discussion

3.1. Characterisation of the salt mixture

DSC analysis was performed to obtain the melting point of the additived Hitec mixture. Figure 2a shows the curve obtained in comparison with the corresponding to pure Hitec salt. According to this curve, the salt mixture melts at 132 ºC, which means that its melting point is 9 ºC below that of Hitec salt (143 ºC)

Regarding the molten salt degradation, the maximum stability temperature was set as the temperature at which 3% of the salt's weight is lost [8]. Based on this criterion, and as it is shown in Fig. 2b, the maximum stability temperature of the prepared ternary salt and Hitec mixture under airflow is 678 ºC and 691 ºC, respectively. These results are in line with the behaviour of the $LiNO_3$ addition found in literature that reveals that the effect of melting point decrease of this compound is also reflected in the degradation temperature [32, 33]

The DSC and TGA results concluded that the working temperature range of the prepared salt mixture is 132 ºC – 678 ºC. Thus, considering these working-temperature-range results, the limitations detected for parabolic-trough CSP plants previously explained and considering information from previous experiments [6, 8, 34], the corrosion test temperature was fixed at 500ºC.

3.2. EIS test

Figure 3 gathers the impedance spectra of 321H substrate obtained at the selected times during the test. As shown, throughout the test the Nyquist plot consisted of a double capacitance loop, indicating that corrosion is controlled by ion transport in the scale, and pointing to the presence of a protective-layer mechanism [35].

The equivalent circuit shown in Fig. 4 aims to represent the phenomena occurring due to the interaction of 321H steel and the additived Hitec molten salt. R_e symbolises the resistance of the electrolyte that in this case corresponds to the molten salt mixture. C_{dl} is the capacitance of the electrical double layer at the steel-melt interface. This element always appears whenever an electrochemical surface exists [36]. R_t represents the charge transference resistance while R_{ox} corresponds to the ions transfer resistance along the oxide layer. C_{ol} is the capacitance of the oxide layer. The charge transference resistance

is relevant at high frequency values while it is negligible at low frequencies where the transportation resistance of ions is dominant [37]. It is common for the EIS experiments that capacitors do not behave ideally. There are several theories regarding the cause of this deviation, e.g. surface roughness, non-uniform current distribution or varying thickness or composition of the oxide scale [38]. To avoid this non-ideal behaviour, without dependence on its origin, constant phase elements (CPE) were used in the equivalent circuits instead of C_{dl} and C_{ol} pure capacitors. In Table 2, C_t and C_{ox} are the modulus values of the two constant phase elements and n_t and n_{ox} are their respective indices [37, 39, 40]. Therefore, according to the equivalent circuit, at 500 °C, 321H stainless steel in molten nitrate-nitrite forms a protective oxide film on its surface [25, 27, 37].

Although the behaviour of the system during the whole experiment may be described through the same equivalent circuit, the impedance spectra clearly shows variations in how the corrosion mechanism progresses throughout the test. The behaviour observed during the initial stages seems to be quite different from that observed between 168 hrs and 1000 hrs. To facilitate discussion around these variations and evaluate the possible causes, Table 2 compiles the electrochemical parameters evaluated by fitting the impedance spectra based on the equivalent circuit shown in Fig. 4.

The fitting parameters listed in Table 2 show that after the initial stages of the corrosion test (from 72 hrs), R_{ox} (oxide layer resistance) diminishes sharply, from ~84 Ω to 25 Ω. This means that, in line with previous discussions [25, 39], the protective behaviour of the formed oxide layer deteriorates as the test progresses from its initial stages.

Furthermore, it was observed that during the initial stages of the test, the value of R_{ox} is bigger than that of R_t (charge transfer resistance). This result is consistent with the initial stages of the test and further indicates that the first oxide layer that forms at the beginning of the corrosion process is high protective. During this initial period, the species diffusion through this layer constitutes the rate-limiting process. However, after these initial stages (beyond 168 hrs), this scenario changes and the R_t value becomes bigger than the R_{ox} value, signifying that the oxide layer formed is less protective than the one formed during the initial stages. Once again, this is in line with previous discussions [25, 39]. Additionally, R_t increases slightly between 168 hrs and 1000 hrs, indicating an increase in the resistance of the charged ions layer (electrical double layer). This behaviour is directly related to the increase in the number of species arisen from the substrate to the molten salt, and mainly to the increase in Cr content, which is highly soluble in the salt [39, 41]. The increase in Cr content in the additived salt was confirmed by performing chemical analyses after the 1000 h of testing (see Table 3). Results showed a higher increase in Cr (54 ppm) compared to the Fe content (9 ppm), which confirms the higher solubility of Cr species in the salt.

With regard to the values of n_t and n_{ox}, it was observed that both parameters decrease after the initial stage of the test (after 168 hrs). They are initially closer to 1. A value near to 1 indicates that the system is behaving as an ideal capacitor [42]. The formation of the initial non-protective corrosion layer could lead to non-homogenous layer thickness that difficult the current distribution. This could explain the evolution of n_t and n_{ox} values.

Finally, it is important to highlight the R_e parameter, which represents the resistance of the molten salt. As shown in Table 2, this parameter remains stable at around 3 Ω throughout the first 72 hrs of the test, which is in line with the values obtained in other nitrate salt mixtures, mainly in the presence of nitrites [26]. However, after this first

period, the value increases sharply to 21.32 Ω and remains more or less constant until the end of the test (around 23 Ω). This increase is related to the instability of the salt and changes in its composition, which is a particular feature of the Hitec salt [43, 44] used as the base salt for this work. Instead of R_e, Fig. 5 shows the value of the electrical conductivity (κ) of the electrolyte. The electrical conductivity was obtained from the electrical resistance (R_e) using equations 3 and 4:

$$R_e = \frac{l}{\mathrm{A}} \cdot \rho \tag{3}$$

$$\kappa = \frac{1}{\rho} \tag{4}$$

where ι is the gap between the electrodes (10 mm), A is the surface area of each electrode in contact with the molten salt (12.6 mm^2), and ρ is the electrical resistivity.

The evolution of the electrical conductivity, gathered in Fig. 5, indicates that after the first 168 h of testing, this parameter remains stable. This could be explained by the system reaching a steady state regarding the charged species that diffused from the molten mixture to the steel and vice versa.

3.2.1. Estimation of the corrosion rate

As previously reported [25], the Stern-Geary equation [45], and the ASTM-G102 Standard Practice [46] were used to estimate the corrosion rate of the material. This methodology assumes that the corrosion attack occurs uniformly across the area of the electrode exposed to the molten salt [25]. The calculation may be expressed as follows:

$$i_{corr} = \frac{I_{corr}}{A} = \frac{B}{R_p} \tag{5}$$

Where i_{corr} is the corrosion's current density ($\mu A \cdot cm^{-2}$), I_{corr} is the total anodic current (μA), A is the exposed area (cm^2), B is the Stern-Geary constant (V), and R_p is the polarisation resistance (Ω). While R_p may be determined from the impedance spectra (see EIS spectrum after 1000 hrs of testing in Fig. 3), since Z_r is the sum of R_p and R_e, the Stern-Geary constant (B) may be calculated as follows:

$$B = \frac{\beta a \cdot \beta c}{2.303 \cdot (\beta a + \beta c)} \quad (6)$$

where βa is the slope of the anodic Tafel reaction, and βc is the slope of the cathodic Tafel reaction.

Once the current density (i_{corr}) is calculated, Faraday's Law can be used to calculate the corrosion rate in terms of penetration rate:

$$v_{corr} = K \frac{i_{corr}}{\rho} EW \quad (7)$$

where $K = 3.27 \cdot 10^{-3}$ $\mu g \cdot \mu A^{-1} \cdot cm^{-1} \cdot yr^{-1}$, EW is the equivalent weight (25.3) and ρ is the density of 321H (7.94 $g \cdot cm^{-3}$).

Table 4 gathers the corrosion rate determined from the EIS test results after 1000 hrs of testing, including the electrochemical parameters aforementioned, the former being of 8.9 $\mu m \cdot year^{-1}$. This value is similar to that measured by Gomes et al. [47], who performed corrosion tests with AISI 321H immersed in a stagnant isothermal mixture of 60% $NaNO_3$ and 40% KNO_3 molten salt at 550 °C in atmospheric air, estimating a corrosion rate of 9.0 $\mu m \cdot year^{-1}$ according to the descaled data. The calculated value is also in the same order of magnitude as Kruizenga and Gill's [23] calculation for this alloy, who obtained a value of 7.1 $\mu m \cdot year^{-1}$ based on 3064 h of exposure to Solar Salt at 500 ºC. Federsel et al. [24] studied the corrosion behaviour of 321H steel in pure Hitec salt at 530 ºC for 2000

hrs obtaining an experimental corrosion rate value of 18 μm·year^{-1}. These results, found in the literature and gathered in Table 5, would confirm that the corrosion behaviour of the additived Hitec is in line with the values registered for the commercial molten salt mixtures.

The evolution of the corrosion rate over time is gathered in Fig. 6. The corrosion rate values have been calculated as an average from the results of three EIS measurements at each monitored time. Results showed a very low dispersion confirming the measurement stability of the method. The evolution of the corrosion rate (see Fig. 6) presents the highest value at the beginning of the 321H steel exposure to the molten salt. As the corrosion layer grows it provides some protection that results in a corrosion rate decrease and ultimately it remains constant. This result is in line with that obtained by Gomes et al. for the corrosion behaviour of 321H steel immersed in Solar Salt [47].

3.3. Corrosion test

As previously described, samples exposed to the gravimetric test were taken in triplicate at the same exposure times than the electrochemical experiment: 0, 24, 72, 168, 250, 500, 750, and 1000 hours, with three specimens being removed from the prepared salt mixture at each interval.

Figure 7 shows the changes to the gravimetric mass of the 321H steel. Initially, the mass of the samples decreased slightly, reaching a mass loss of -0.0225 mg·cm^{-2} after 168 hrs of testing. This initial behaviour may be related to the formation of a protective surface oxide film with Cr_2O_3 as its main component. Given the high solubility of Cr in the salt, as the Cr_2O_3 forms, it continuously dissolves as chromates (CrO_4^{2-}) in the mixture [48], which would explain this initial gravimetric behaviour. Then, between 168 hrs and 500 hrs of testing, the gravimetric curve indicates fluctuations in mass gain, possibly due

to the formation of non-adherent corrosion products that become detached during the test, such as iron oxides [49]. Iron in the steel can rapidly be oxidized to form Fe_2O_3 and Fe_3O_4 oxide film, which is loose and porous and has no protective ability. Fe-based oxides have some solubility in molten salt, which results in the formation of a fast-growing non-protective porous oxide scale [48]. Finally, the mass increases steadily until the end of the test (0.1907 $mg \cdot cm^{-2}$), which may indicate the presence of more adherent corrosion layers (probably Fe-Cr spinels). Spallation of oxide scales on stainless-steel surfaces has been previously reported [47, 50, 51]. Trent et al. affirmed that the spallation is the result of increased stress due to the mismatch between the thermal expansions of the steel and corrosion scale during cooling [50]. Moreover, Scott and Wei confirmed that the detachment of the oxide scales may also occur in situ, which leads to iron oxide re-growth [51].

In order to confirm all the above speculations, further results based on SEM and XRD analyses are needed. Figure 8 shows the appearance of a cross-section of the samples obtained by SEM after 1000 hrs of testing. This micrograph clearly shows a corrosion layer of 5.58 ± 1.06 μm growing on the substrate. According to the EDX analysis (see Fig. 9), the corrosion band has a multi-layered structure, with the upper layers being iron oxides, and the inner layers being chromium-iron oxides. These results were confirmed by XRD analysis (see Fig. 10), which indicated a corrosion layer composed of Fe_2O_3 and $FeCr_2O_4$. The results are in line with that observed in the gravimetric curves.

Furthermore, to confirm the formation of Cr_2O_3 during the first stages of the corrosion test, XRD analysis was carried out on the 321H samples after 168 hrs of testing. The XRD analysis (grazing-incidence angle) shown in Fig. 11 clearly reveals the presence of this species, which is then lost because of its high solubility in molten nitrates. This result

confirms the observations taken from the gravimetric curve in Fig. 7 and from the evolution of the corrosion rate over time, as is shown in Fig. 6.

It is important to remark that lithium was not detected in the corrosion products. Several researchers have reported lithiumization as one of the main corrosion processes when steels were exposed to nitrate mixtures containing $LiNO_3$ [49, 52-55]. The higher basicity of $LiNO_3$ in comparison with potassium and sodium nitrates suggests that the steels are preferentially attacked by Li^+ ions [56]. The lithiumization mechanism proceeds via (1) to (3) reactions [52, 56]:

$$Fe^{3+}+Li^{+}+2O^{2-}\rightarrow LiFeO_2 \quad (1)$$

$$6Fe_2O_3+2Li^{+}\rightarrow 2LiFe_5O_8+2Fe^{3+}+2O^{2-} \quad (2)$$

$$LiFe_5O_8+3Li^{+}\rightarrow 4LiFeO_2+Fe^{3+} \quad (3)$$

Due to the low atomic number of the lithium, it is not possible to detect it by EDX. Therefore, XRD results were thoroughly analysed in order to assess the presence of lithium oxides. Standard patterns of $LiFeO_2$ and $LiFe_5O_8$, compiled by JCPDS Committee, were compared to the 321H diffraction pattern after molten salt exposure with no success. To the best of the authors knowledge, studies found in literature that reports lithiumization mechanism in nitrate molten salts refers to mixtures with weight percentage in $LiNO_3$ above 10% [49, 52-54]. Based on this fact, it is supposed that the lack of lithium species in this study could be explained by the low content of $LiNO_3$ (1 w%) in the mixture. However, to confirm this hypothesis, it will be needed to perform further studies focused on the lithium concentration in the corrosive media.

4. Conclusions

This research assessed and monitored the corrosive behaviour of 321H alloy when in contact with a Hitec salt to which 1%wt. of $LiNO_3$ was added, by using a corrosion

monitoring system based on electrochemical measurements. Tests were carried out under isothermal conditions at 500 ºC and had a duration of 1000 hours. The proposed corrosion monitoring system was developed and adapted for parabolic trough technology and finally tested at lab-scale. The corrosion monitoring system's results were then validated by conventional characterisation techniques commonly used in the laboratory.

EIS results at lab-scale indicated that corrosion in 321H is controlled by ion transport in the scale, and points to the presence of a protective-layer mechanism. The fitting parameters listed show that, after the initial stages of the corrosion test, R_{ox} diminishes sharply from~84 Ω to 25 Ω, indicating that the protective behaviour of the formed oxide layer deteriorates as the test progresses. Additionally, between 168 hrs and 1000 hrs, R_t increases slightly, indicating an increase in the resistance of the charged ions layer and, therefore, an increase in the number of species arisen from the substrate to the molten salt. Furthermore, the EIS results give an estimated corrosion rate of 8.9 $\mu m \cdot year^{-1}$, which concurs with other reported pieces of research.

The results obtained by the corrosion monitoring system were supported by other conventional techniques. These techniques indicated the formation of a corrosion layer mainly composed of Fe_2O_3 and $FeCr_2O_4$. Moreover, characterisation results also confirmed the formation of Cr_2O_3 during the first stages of the test, which is later solubilised in the molten salt. These results are in line with the conclusions of the EIS results.

Chemical analyses showed a higher increase of the Cr content in the molten salt (54 ppm) compared to the Fe concentration (9 ppm). This fact reveals the preferential solvation of Cr species in the nitrate – nitrite mixture. This phenomenon could have an

important effect in the environmental impact of the salt at the end of the lifetime of the CSP plant when the storage tanks must be cleaned.

The results confirm the suitability of 321H stainless steel as a construction material for parabolic trough CSP technology. The corrosive behaviour of the studied quaternary molten mixture has demonstrated to be similar to the commercial mixtures currently used in CSP plants. Furthermore, the research demonstrates the huge potential of using the corrosion monitoring system to assess the corrosion process in parabolic-trough plants. The next step would be to install a larger-scale model of the proposed system in a demonstration parabolic trough plant, in order to test it under more realistic conditions.

Author statement

V. Encinas-Sanchez: Conceptualization, Validation, Writing – Original Draft, Writing – Review & Editing, Visualization **M.I. Lasanta:** Conceptualization, Methodology, Validation, Investigation, Project administration **M.T. de Miguel:** Conceptualization, Validation, Investigation, Writing – Review & Editing, Visualization, Project administration **G. García-Martín:** Resources, Writing – Review & Editing, Project administration **F.J. Pérez:** Conceptualization, Supervision, Funding acquisition

Acknowledgments

This work received funding from the European Union's Horizon 2020 research and innovation programme under grant agreement No 730609, project *MSLOOP*.

Data Availability

The raw/processed data that support the findings of this study cannot be shared at this time as the data form part of another ongoing study.

References

[1] H. Beidaghy-Dizaji. H. Hosseini, A review of material screening in pure and mixed-metal oxide thermochemical energy storage (TCES) systems for concentrated solar power (CSP) applications, Renewable and Sustainable Energy Reviews 98 (2018) 9-26.

[2] International Energy Agency (IEA). World Energy Outlook 2018, edition 2018.

[3] M.T. de Miguel, V. Encinas-Sánchez, M.I. Lasanta, G. García-Martín, F.J. Pérez, Corrosion resistance of HR3C to a carbonate molten salt for energy storage applications in CSP plants, Solar Energy Materials and Solar Cells 157 (2016) 966-972.

[4] V. Encinas-Sánchez, M.T. de Miguel, G. García-Martín, M.I. Lasanta, F.J. Pérez, Corrosion resistance of Cr/Ni alloy to a molten carbonate salt at various temperatures for the next generation high-temperature CSP plants, Solar Energy 171 (2018) 286-292.

[5] A. Bonk, S. Sau, N. Uranga, M. Hermaiz, T. Bauer, Advanced heat transfer fluids for direct molten salt line-focusing CSP plants, Progress in Energy and Combustion Science 67 (2018) 69-87.

[6] G. García-Martín, M.I. Lasanta, V. Encinas-Sánchez, M.T. de Miguel, F.J. Pérez, Evaluation of corrosion resistance of A516 Steel in a molten nitrate salt mixture using a pilot plant facility for application in CSP plants, Solar Energy Materials and Solar Cells 161 (2017) 226-231.

[7] V.M.B. Nunes, C.S. Queiro, M.J.V. Lourenço, F.J.V. Santos, C.A.N. Castro, Molten salts as engineering fluids-A review: Part I. Molten alkali nitrates, Applied Energy 183 (2016) 603-611.

[8] A.G. Fernández, H. Galleguillos, E. Fuentealba, F.J. Pérez, Thermal characterization of HITEC molten salt for energy storage in solar linear concentrated technology, Journal of Thermal Analysis and Calorimetry, 122 (2015) 3-9.

[9] X. Li, S. Wu, Y. Wang, L. Xie, Experimental investigation and thermodynamic modeling of an innovative molten salt for thermal energy storage (TES) applied Energy 212 (2018) 516-526.

[10] Q. Peng, J. Ding, W. Xiaolan, Y. Jianping, Y. Xiaoxi, The preparation and properties of multi-component molten salts, Applied Energy 87 (2010) 2812–2817.

[11] R. Serrano-López, J. Fradera, S. Cuesta-López, Molten salts database for energy applications, Chemical Engineering and Processing 73 (2013) 87–102.

[12] A.G. Fernández, S. Ushak, H. Galleguillos, F.J. Pérez, Development of new molten salts with $LiNO_3$ and $Ca(NO_3)_2$ for energy storage in CSP plants, Applied Energy 119 (2014) 131–140.

[13] W. Song, Y. Lu, Y. Wu, C. Ma, Effect of SiO2 nanoparticles on specific heat capacity of low-melting-point eutectic quaternary nitrate salt, Solar Energy Materials and Solar Cells 179 (2018) 66-71.

[14] R.W. Bradshaw, D.E. Meeker, High-temperature stability of ternary nitrate molten salts for solar thermal energy systems, Solar Energy Materials 21(1990) 51-60.

[15] B. Dudda, D. Shin, Effect of nanoparticle dispersion on specific heat capacity of a binary nitrate salt eutectic for concentrated solar power applications, International Journal of Thermal Sciences 69 (2013) 37-42.

[16] X.H. Ming, C. Pan, Optimal concentration of alumina nanoparticles in molten Hitec salt to maximize its specific heat capacity, Int. J. Heat Mass Transf., 70 (2014) 174-184.

[17] R.W. Bradshaw, N.P. Siegel, Molten nitrate salt development for thermal energy storage in parabolic trough solar power system, Energy Sustainability, 2008.

[18] J.G. Cordaro, N.C. Rubin, R.W. Bradshaw, Multicomponent molten salt mixtures based on nitrate/nitrite anions, Solar Energy Engineering, 133 (2011).

[19] P. Gauché, J. Rudman, M. Mabaso, W.A. Landman, T.W. von Backström, A.C. Brent, System value and progress of CSP, Solar Energy 152 (2017) 106-139.

[20] W.-D. Steinmann, Advances in thermal energy storage systems - methods and applications; chap. Thermal energy storage systems for concentrating solar power (CSP) technology, Woodhead Publishing (2015) 511-531.

[21] M. Walczak, F. Pineda, A.G. Fernández, C. Mata-Torres, R.A. Escobar, Materials corrosion for thermal energy storage systems in concentrated solar power plants, Renewable and Sustainable Energy Reviews 86 (2018) 22-44.

[22] S. Sau, N. Corsaro, T. Crescenzi, C. D'Ottavi, R. Liberatore, S. Licoccia, V. Russo, P. Tarquini, A.C. Tizzoni, Techno-economic comparison between CSP plants presenting two different heat transfer fluids, Applied Energy 168 (2016) 96-109.

[23] A. Kruizenga, D. Gill, Corrosion of iron stainless steels in molten nitrate salt, Energy Procedia 49 (2014) 878-887.

[24] K. Federsel, J. Wortmann, M. Ladenberger, High-temperature and corrosion behavior of nitrate nitrite molten salt mixtures regarding their application in concentrating solar power plants, Energy Procedia 69 (2015) 618-625.

[25] V. Encinas-Sánchez, M.T. de Miguel, M.I. Lasanta, G. García-Martín, F.J. Pérez, Electrochemical impedance spectroscopy (EIS): An efficient technique for monitoring corrosion processes in molten salt environments in CSP applications, Solar Energy Materials and Solar Cells 191 (2019) 157-163.

[26] Y. Han, J. Wang, H. Zhang, S. Zhao, Q. Ma, Z. Wang, Electrochemical impedance spectroscopy (EIS): An efficiency method to monitor resin curing processes, Sensors and Actuators A: Physical 150 (2016) 78-86.

[27] C.L. Zeng, W. Wang, W.T. Wu, Electrochemical impedance models for molten salt corrosion, Corrosion Science 43 (2001) 787-801.

[28] Y. Liu, Q. Chen, K. Hu, J. Hao, Flow field optimization for the solar parabolic trough receivers in direct steam generation systems by the variational principle. International Journal of Heat and Mass Transfer 102 (2016) 1073-1081.

[29] W. Fuqiang, C. Ziming, T. Wianyu, Y. Yuan, L. Yong-Shuai, Progress in concentrated solar power technology with parabolic trough collector system: A

comprehensive review. Renewable and Sustainable Energy Reviews 79 (2017) 1314-1328.

[30] V. Encinas-Sánchez, E. Batuecas, A. Macías-García, C. Mayo, R. Díaz, F. J. Pérez, Corrosion resistance of protective coatings against molten nitrate salts for thermal energy storage and their environmental impact in CSP technology, Solar Energy 176 (2018) 688-697.

[31] F.J. Pérez, D. Duday, M.P. Hierro, C. Gómez, M. Romero, M.T. Casais, J.A. Alonso, M.J. Martínez, L. Daza, Analysis by electrochemical impedance spectroscopy of new MCFC cathode materials. Journal of Power Sources, 86 (2000) 309-315.

[32] C.Villada, F. Jaramillo, J. G. Castaño, F. Echeverría, F. Bolívar, Design and development of nitrate-nitrite based molten salts for concentrating solar power applications, Solar Energy, 188 (2019) 291-299.

[33] T. Wang, D. Mantha, R. G. Reddy (2013). Novel low melting point quaternary eutectic system for solar thermal energy storage. Applied Energy, 102 (2013) 1422-1429

[34] M. Liu, N.H.S. Tay, S. Bell, M. Belusko, R. Jacob, G. Will, W. Saman, F. Bruno, Review on concentrating solar power plants and new developments in high temperature thermal energy storage technologies, Renewable and Sustainable Energy Reviews 53 (2016) 1411-1432.

[35] K. Beaussant-Törne, A. Örnberg, J. Weissenrieder, Characterization of the protective layer formed on zinc in whole blood, Electrochimica Acta 258 (2017) 1476-1483.

[36] R. G. Kelly, J.R. Scully, D.W. Shoesmith, R.G. Buchheit, (2003) Electrochemical Techniques in Corrosion Science and Engineering, New York, USA. Marcel Dekker, Inc.

[37] Pérez, F. J., Hierro, M. P., Nieto, J., Waste incineration corrosion processes: Oxidation mechanisms by electrochemical impedance spectroscopy, Materials and Corrosion 59 (2008) 566-572

[38] Gamry Instruments, Basics of Electrochemical Impedance Spectroscopy (https://www.gamry.com/application-notes/EIS/basics-of-electrochemical-impedance-spectroscopy/) Accessed on May 10, 2020.

[39] M. Zhu, S. Zeng, H. Zhang, J. Li, B. Cao, Electrochemical study on the corrosion behaviors of 316 SS in HITEC molten salt at different temperatures, Solar Energy Materials and Solar Cells 186 (2018) 200-207.

[40] C. S. Ni, L. Y. Lu, Electrochemical Impedance and Modelling Studies of the Corrosion of Three Commercial Stainless Steels in Molten Carbonate, International Journal of Corrosion (2014) 1-13.

[41] P. Audigié, V. Encinas-Sánchez, M. Juez-Lorenzo, S. Rodríguez, M. Gutiérrez, F.J. Pérez, A. Agüero, High temperature molten salt corrosion behavior of aluminide and nickel-aluminide coatings for heat storage in concentrated solar power plants, Surface and Coatings Technology 349 (2018) 1148-1157.

[42] S. Omar, F. Repp, P.M. Desimone, R. Weinkamer, W. Wagermaier, S. Ceré, J. Ballarre, Sol–gel hybrid coatings with strontium-doped 45S5 glass particles for

enhancing the performance of stainless steel implants: Electrochemical, bioactive and in vivo response, Journal of Non-Crystalline Solids 425 (2015) 1-10.

[43] P. Gimenez, S. Fereres, Effect of heating rates and composition on the thermal decomposition of nitrate based molten salts, Energy Procedia 69 (2015) 654-662.

[44] C. Villada, A. Bonk, T. Bauer, F. Bolívar, High-temperature stability of nitrate/nitrite molten salt mixtures under different atmospheres, Applied Energy 226 (2018) 107-115.

[45] V. Encinas-Sánchez, A. Macías-García, M.A. Díaz-Díez, P. Brito, D. Cardoso. Influence of the quality and uniformity of ceramic coatings on corrosion resistance, Ceram. Int. 41 (2015) 5138-5146.

[46] ASTM G102 – Standard Practice for Calculation of Corrosion Rates and Related Information from Electrochemical Measurements, 1994.

[47] A. Gomes, M. Navas, N. Uranga, T. Paiva, I. Figueira, T.C. Diamantino, High-temperature corrosion performance of austenitic stainless steels type AISI 316L and AISI 321H, in molten Solar Salt, Solar Energy 177 (2019) 408-419.

[48] M. Zhu, S. Zeng, H. Zhang, J. Li, B. Cao, Electrochemical study on the corrosion behaviors of 316 SS in HITEC molten salt at different temperatures, Solar Energy Materials and Solar Cells 186 (2018) 200-207.

[49] A.G. Fernández, F.J. Pérez, Improvement of the corrosion properties in ternary molten nitrate salts for direct energy storage in CSP plants, Solar Energy 134 (2016) 468-478.

[50] M.C. Trent, S.H. Goods, R.W. Bradshaw, Comparison of corrosion performance of grade 316L and grade 347H stainless steels in molten nitrate salt, AIP Conference Proceedings, 1734 (2016) 160017-1–160017-12.

[51] F.H. Scott, F.I. Wei, High temperature oxidation of commercial austenitic stainless steels. Materials science and technology, 5 (1989) 1140–1147.

[52] Cheng, W.-J., Chen, D.-J., Wang, C.-J. High-temperature corrosion of Cr–Mo steel in molten $LiNO_3$–$NaNO_3$–KNO_3 eutectic salt for thermal energy storage. Solar Energy Materials and Solar Cells 132 (2015) 563-569.

[53] A.G. Fernández, L.F. Cabeza, Molten salt corrosion mechanisms of nitrate based thermal energy storage materials for concentrated solar power plants: A review, Solar Energy Materials and Solar Cells, 194 (2019) 160-165

[54] A.G. Fernandez, H. Galleguillos, F. J. Pérez, Corrosion Ability of a Novel Heat Transfer Fluid for Energy Storage in CSP Plants. Oxidation of Metals 82 (2014) 331-345.

[55] W. Xie, J. Ding, X. Wei, W. Wang, G. Xia, J. Xing, Corrosion Resistance of Stainless Steel and Pure Metal in Ternary Molten Nitrate for Thermal Energy Storage, Energy Procedia 158 (2019) 4897-4902.

[56] Spiegel, M., P. Biedenkopf, H. J. Grabke, Corrosion of iron base alloys and high alloy steels in the Li_2CO_3-K_2CO_3 eutectic mixture. Corrosion Science, 39 (7) (1997) 1193-1210.

Figure captions

Figure 1. Sketch of the experimental setup for corrosion monitoring.

Figure 2. Characterisation of the salt mixture: (a) differential scanning calorimetry; and (b) thermogravimetric analysis.

Figure 3. Impedance spectra of 321H steel tested at 500 ºC in the quaternary salt mixture for 1000 hrs.

Figure 4. Equivalent circuit for a protective-layer mechanism.

Figure 5. Evolution of the electrical conductivity (κ) of the electrolyte throughout the test.

Figure 6. Evolution of the average corrosion rate over time for 321H steel in contact with the quaternary salt mixture at 500 ºC for 1000 hours.

Figure 7. Gravimetric analysis of the 321H specimens after 1000 hours in contact with the quaternary salt mixture at 500 ºC.

Figure 8. BSE cross-section image at 25 kV and x5000 magnification. SEM micrographs of a 321H specimen after 1000 hours at 500 ºC. Magnification: x 5000.

Figure 9. BSE cross-section image at 25 kV and x5000 magnification. EDX analysis of a 321H specimen after 1000 hours at 500 ºC.

Figure 10. XRD analysis of a 321H specimen after 1000 hours at 500 ºC.

Figure 11. XRD analysis of a 321H specimen after 168 hours of testing, using grazing-incidence angle.

Tables

Table 1. Impurities concentration in the quaternary molten salt mixture

Hitec + 1%$LiNO_3$					
Chlorides ($\mu g \cdot g^{-1}$)	**Sulphates ($\mu g \cdot g^{-1}$)**	**Carbonates ($\mu g \cdot g^{-1}$)**	**Magnesium ($\mu g \cdot g^{-1}$)**	**Aluminium ($\mu g \cdot g^{-1}$)**	**Calcium ($\mu g \cdot g^{-1}$)**
122 ± 7	431 ± 43	< 600	< 1	< 1	25 ± 2

Table 2. Electrochemical parameters evaluated by fitting the impedance spectra.

	Equivalent circuit - Porous layer						
Time, h	**24**	**72**	**168**	**250**	**500**	**750**	**1000**
R_e, Ω	3.019	2.953	21.32	19.75	21.8	23.51	23.03
C_t, F	$1.51 \cdot 10^{-2}$	$4.21 \cdot 10^{-2}$	$5.11 \cdot 10^{-3}$	$2.24 \cdot 10^{-3}$	$7.49 \cdot 10^{-3}$	$8.29 \cdot 10^{-3}$	$8.45 \cdot 10^{-3}$
n_t	1.031	1.087	0.498	0.510	0.518	0.549	0.545
R_t, Ω	1.68	0.670	297.8	217.84	305.9	337.9	420.8
C_{ox}, F	$1.47 \cdot 10^{-2}$	$1.99 \cdot 10^{-2}$	$2.41 \cdot 10^{-3}$	$1.57 \cdot 10^{-3}$	$9.25 \cdot 10^{-4}$	$6.95 \cdot 10^{-4}$	$6.63 \cdot 10^{-3}$
n_{ox}	0.466	0.410	0.599	0.664	0.647	0.646	0.648
R_{ox}, Ω	71.32	84.33	25.2	11.98	23.34	25.67	23.09

Table 3. Variation in Fe and Cr content in the salt after 1000 hours of test.

Time, h	**Fe, ppm**	**Cr, ppm**
0	<1	<1
1000	9	54

Table 4. Corrosion rate determined from the EIS test results.

Time, h	**Z_r (R_e+R_p)**	**R_e, Ω**	**R_p, Ω**	**i_{corr}, $\mu A\ cm^{-2}$**	**v_{corr}, $\mu m\ year^{-1}$**
1000	53.7	23	30.7	847.3	8.9

Table 5. Corrosion rate of 321H steel in commercial molten salt mixtures

Steel	Molten salt	Temperature (ºC)	Time (h)	Corrosion rate (μm·year^{-1})	Reference
321H	Hitec + 1% LiNO3	500	1000	8.9	This study
321H	Hitec	530	2000	18	[24]
321H	Solar Salt	500	3000	7.1	[23]
321H	Solar Salt	550	3000	9	[47]
321H	Solar Salt	600	3000	15.9	[23]

Table 6. Angle (2θ (º)) and lattice plane parameters (hkl) of the crystalline compounds identified by XRD in a 321H specimen after 1000 hours at 500 ºC. Reference code corresponds to the standard pattern from JCPDS Committee.

Fe_2O_3 (Reference code: 00-039-1346)			
h	**k**	**l**	**2θ (º)**
2	2	0	30,241
3	1	1	35,631
4	0	0	43,285
5	1	1	57,273
4	4	0	62,927
5	3	3	74,473

$FeCr_2O_4$ (Reference code: 01-080-6393)			
h	**k**	**l**	**2θ (º)**
2	2	2	30,127
3	1	1	35,486
2	2	2	37,121
4	0	0	43,128
5	1	1	57,038
4	4	0	62,636
5	3	3	74,104

Table 7. Angle (2θ (º)) and lattice plane parameters (hkl) of the crystalline compounds identified by XRD in a 321H specimen after 168 hours at 500 ºC. Reference code corresponds to the standard pattern from JCPDS Committee.

Fe_2O_3 (Reference code: 00-039-1346)			
h	**k**	**l**	**2θ (º)**
2	2	0	30,241
3	1	1	35,631
4	0	0	43,285
5	1	1	57,273
4	4	0	62,927
5	3	3	74,473

$FeCr_2O_4$ (Reference code: 01-080-6393)			
h	**k**	**l**	**2θ (º)**
2	2	2	30,127
3	1	1	35,486
2	2	2	37,121
4	0	0	43,128
5	1	1	57,038
4	4	0	62,636
5	3	3	74,104

Cr_2O_3 (Reference code: 00-006-0504)			
h	**k**	**l**	**2θ (º)**
0	1	2	24,482
1	0	4	33,588
1	1	0	36,191
0	0	6	39,783
1	1	3	41,464
2	0	2	44,187
0	2	4	50,197
1	1	6	54,865
2	1	4	63,444
3	0	0	65,115
1	0	10	72,928
3	0	6	79,071
3	1	2	82,088
0	2	10	84,215

Figures

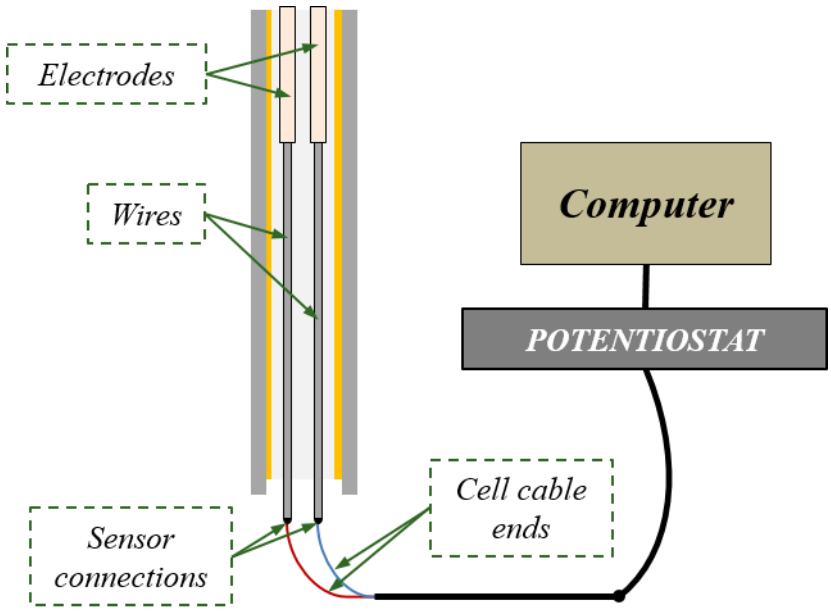

Figure 1

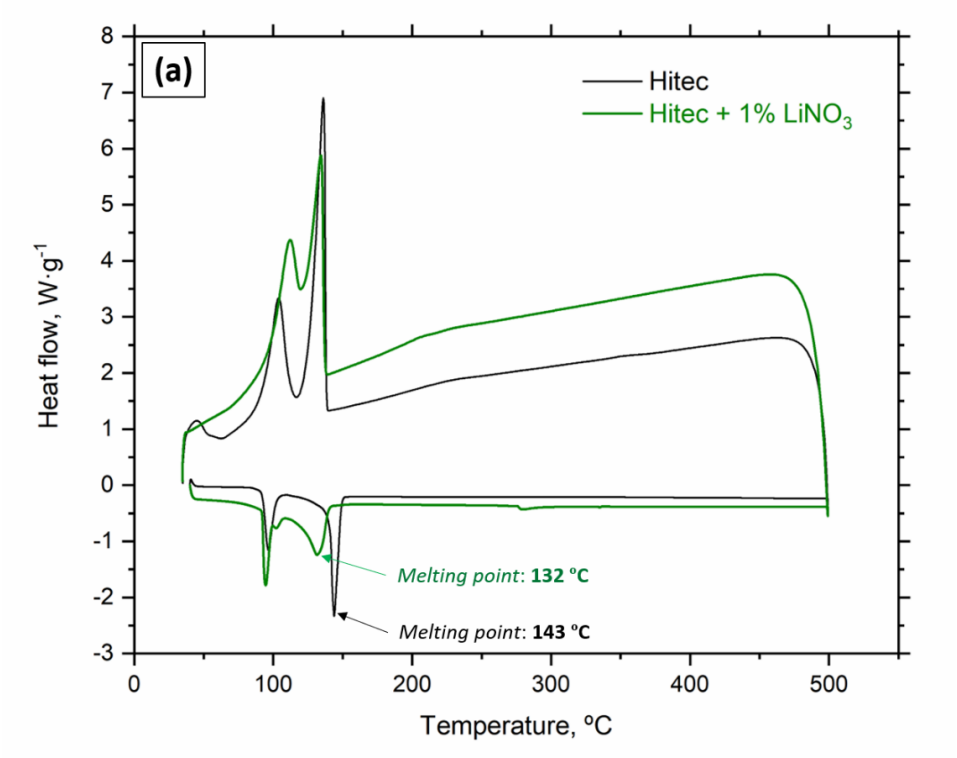

Figure 2a

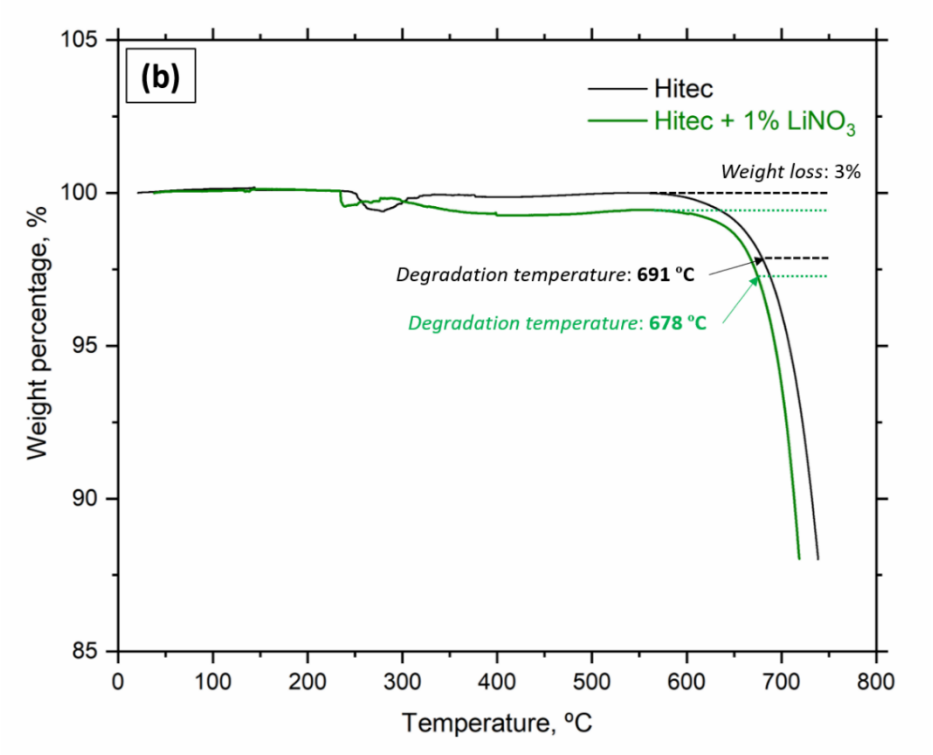

Figure 2b

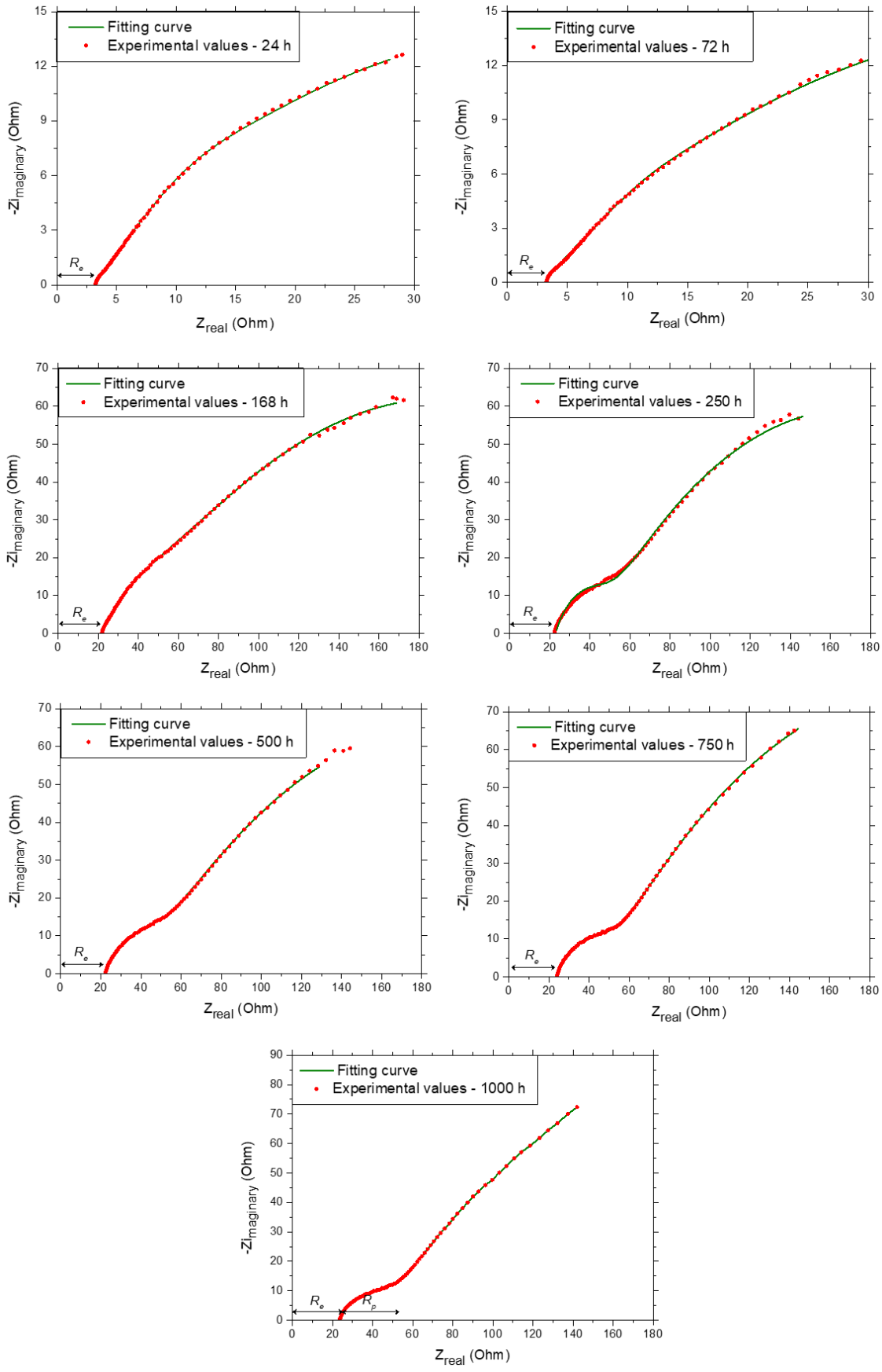
Fitting curve
Experimental values - 24 h
Experimental values - 72 h
Experimental values - 168 h
Experimental values - 250 h
Experimental values - 500 h
Experimental values - 750 h
Experimental values - 1000 h
R_e
R_p
$-Z_{imaginary}$ (Ohm)
Z_{real} (Ohm)

Figure 3

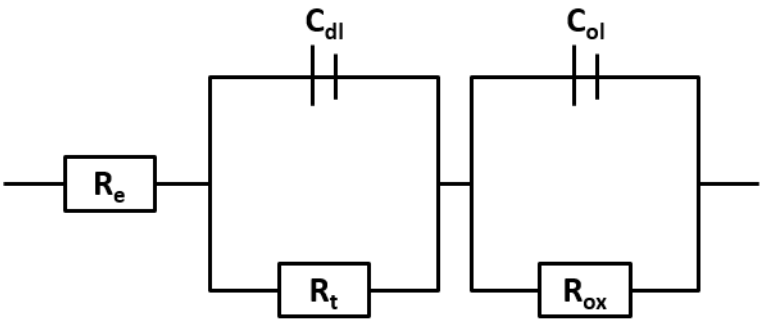

Figure 4

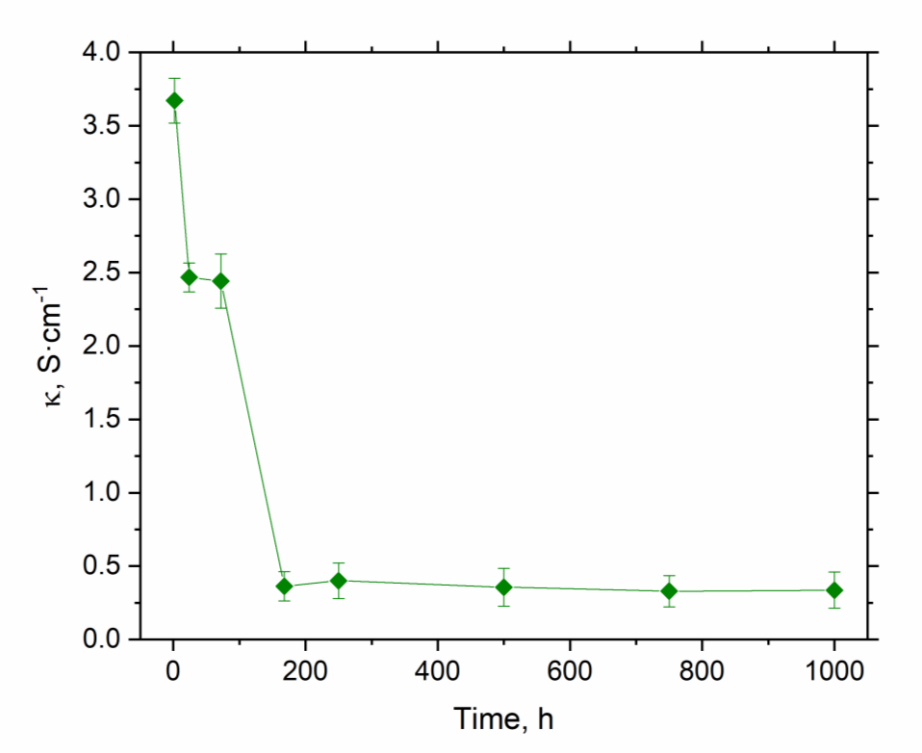

Figure 5

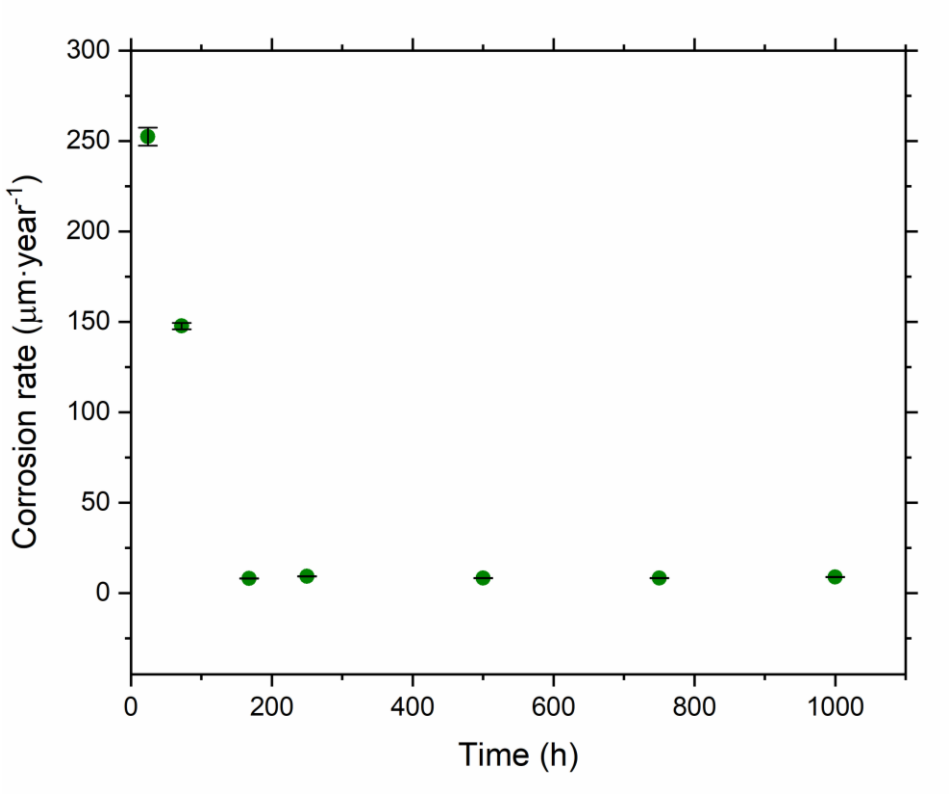
Corrosion rate (μm·year-1)
300
250
200
150
100
50
0
0
200
400
600
800
1000
Time (h)

Figure 6

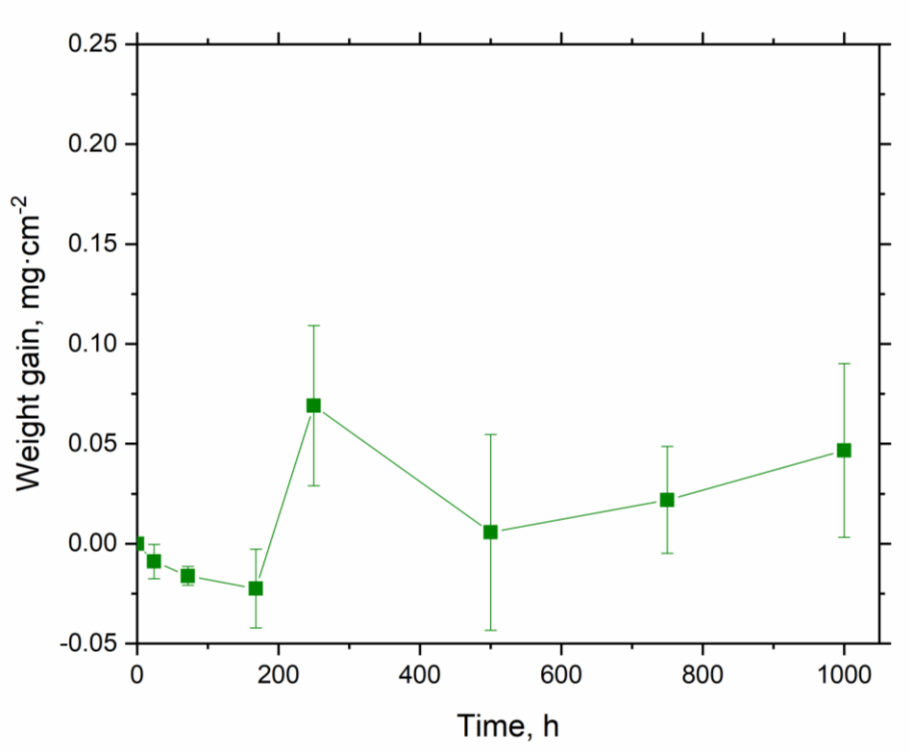
0.25
0.20
0.15
0.10
0.05
0.00
-0.05
Weight gain, mg·cm-2
0
200
400
600
800
1000
Time, h

Figure 7

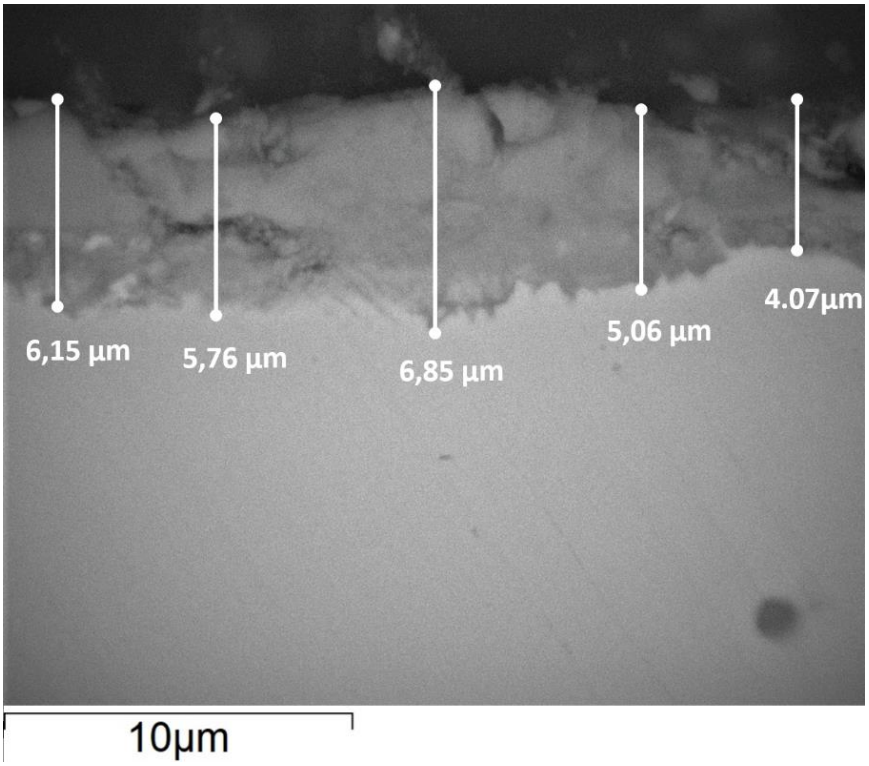

Figure 8

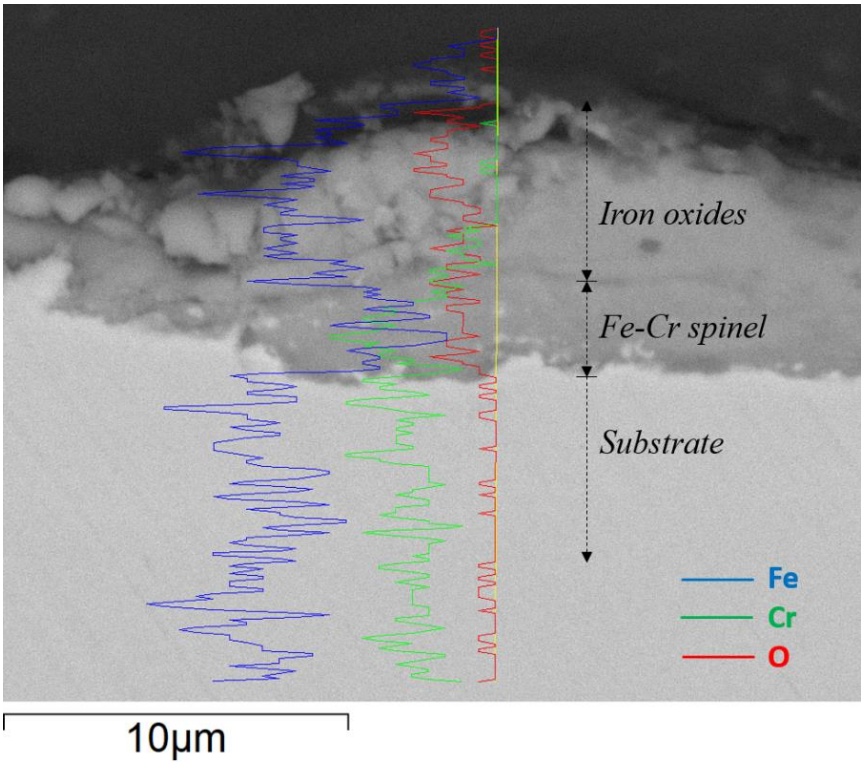

Figure 9

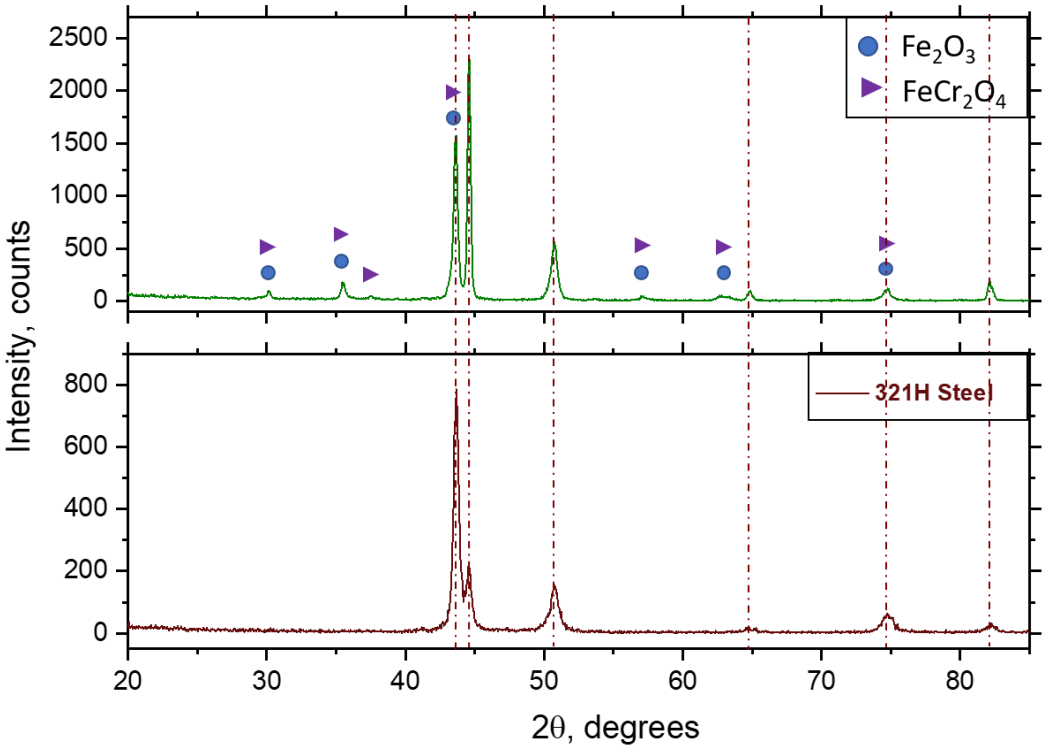
Fe2O3
FeCr2O4
321H Steel
Intensity, counts
2θ, degrees
2500
2000
1500
1000
500
0
800
600
400
200
0
20
30
40
50
60
70
80

Figure 10

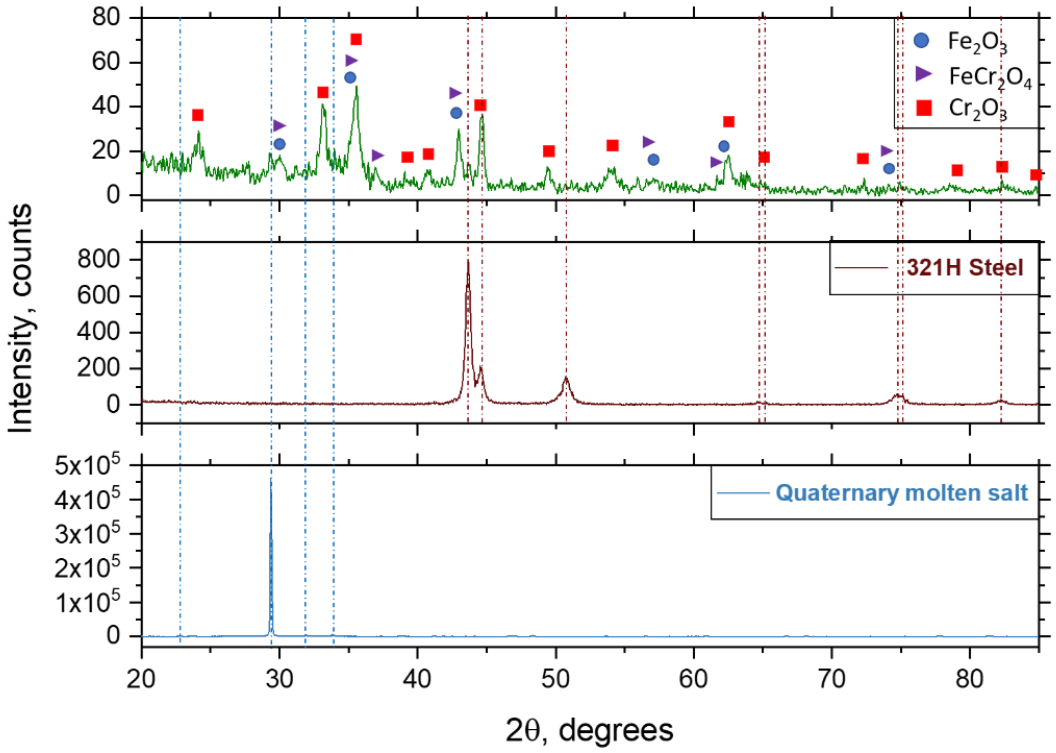
Intensity, counts
2θ, degrees
Fe2O3
FeCr2O4
Cr2O3
321H Steel
Quaternary molten salt

Figure 11

Declaration of interests

☐ The authors declare that they have no known competing financial interests or personal relationships that could have appeared to influence the work reported in this paper.

☒The authors declare the following financial interests/personal relationships which may be considered as potential competing interests:

Ángel G. Fernández (GREiA Research Group INSPIRES Research Centre, Lleida University and Energy Development Center, **University of Antofagasta**)

Luisa F. Cabeza (GREiA Research Group INSPIRES Research Centre, **University of Lleida**)

Héctor R. Galleguillos (Chemical Engineering and Mining Processes Department, **University of Antofagasta**)

Edward Fuentealba (Chemical Engineering and Mining Processes Department, **University of Antofagasta**)

Cristina Prieto (**Abengoa** and **University of Sevilla**)

F. Javier Ruiz-Cabañas (**Abengoa** and **University of Sevilla**)

Author statement

V. Encinas-Sanchez: Conceptualization, Validation, Writing – Original Draft, Writing – Review & Editing, Visualization **M.I. Lasanta:** Conceptualization, Methodology, Validation, Investigation, Project administration **M.T. de Miguel:** Conceptualization, Validation, Investigation, Writing – Review & Editing, Visualization, Project administration **G. García-Martín:** Resources, Writing – Review & Editing, Project administration **F.J. Pérez:** Conceptualization, Supervision, Funding acquisition